Nanomechanical detection of itinerant electron spin flip

GUITI ZOLFAGHARKHANI[1], ALEXEI GAIDARZHY[2], PASCAL DEGIOVANNI[1,3], STEFAN KETTEMANN[4], PETER FULDE[5] AND PRITIRAJ MOHANTY[1]*

[1]Department of Physics, Boston University, 590 Commonwealth Avenue, Boston, Massachusetts 02215, USA
[2]Department of Mechanical and Aerospace Engineering, Boston University, 110 Cummington Street, Boston, Massachusetts 02215, USA
[3]Université de Lyon, Fédération de Physique André Marie Ampère, CNRS-Laboratoire de Physique de l'Ecole Normale, Supérieure de Lyon, 46 Allée d'Italie, 69364 Lyon Cedex 07, France
[4]Jacobs University Bremen, School of Engineering and Science, Campus Ring 1, D-28759 Bremen, Germany
[5]Asia Pacific Centre for Theoretical Physics, Namgu Pohang, Gyeongbuk 790-784, Korea
*e-mail: mohanty@physics.bu.edu

Published online: 2 November 2008; doi:10.1038/nnano.2008.311

Electrons and other fundamental particles have an intrinsic angular momentum called spin. A change in the spin state of such a particle is therefore equivalent to a mechanical torque. This spin-induced torque is central to our understanding of experiments[1,2] ranging from the measurement of the angular momentum of photons[3] and the *g*-factor of metals[4–7] to magnetic resonance[8] and magnetization reversal in magnetic multilayers[8–15]. When a spin-polarized current passes through a metallic nanowire in which one half is ferromagnetic and the other half is nonmagnetic, the spins of the itinerant electrons are 'flipped' at the interface between the two regions to produces a torque. Here, we report direct measurement of this mechanical torque in an integrated nanoscale torsion oscillator, and measurements of the itinerant electron spin polarization that could yield new information on the itinerancy of the *d*-band electrons. The unprecedented torque sensitivity of 1×10^{-22} N-m Hz$^{-1/2}$ may have applications in spintronics and precision measurements of charge–parity-violating forces[16,17], and might also enable experiments on the untwisting of DNA[18] and torque-generating molecules[19,20].

Extensive studies of spin transfer and spin relaxation at a ferromagnetic–nonmagnetic (FM–NM) interface[21–23] have shown that such a system can act as an effective source or sink of angular momentum in the presence of an electric current[24,25]. Consider a device involving a hybrid metallic nanowire with a FM left half and a NM right half (Fig. 1a). Because the ferromagnet is magnetized by an axial magnetic field B along the wire, this arrangement allows spin polarization in the FM segment and spin flip at the interface between the two segments of the nanowire[26]. When a current I is driven through the wire, a non-equilibrium spin density accumulation $\delta m = \mu_B \Delta N_{noneq}/V = \mu_B (I_s/e)(\tau_{sf}/V)$ is produced near the FM–NM interface as a result of the balance between spin-injection and spin-relaxation processes[22]. Here, μ_B is the Bohr magneton, V is the volume, τ_{sf} is the spin relaxation time and ΔN_{noneq} is the number of non-equilibrium spins. The spin-polarized injection current is $I_s = I_{up} - I_{down} = P_I \times I$, where $P_I = (I_{up} - I_{down})/I$.

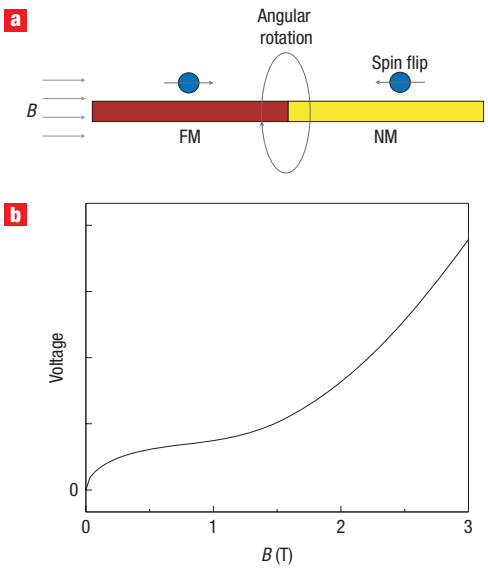

Figure 1 The spin-torsion mechanism. a, At the interface of the ferromagnetic (FM) and nonmagnetic (NM) segments of a quasi-one-dimensional nanowire, the spin-polarized charge carriers undergo spin relaxation. An external magnetic field B is applied to magnetize the ferromagnet along the easy axis. The change in the spin direction of the electrons produces a mechanical torque (directed along the wire) on the crystal lattice and angular rotation of the wire as a result of the conservation of angular momentum. **b**, Analytical form of the expected voltage signal (amplitude of equation (2) in the text). The evidence for the spin torque is the deviation of the response from the B^2 Lorentz form.

Therefore, the spin-flip transfer torque is given by[24,26]

$$\vec{T}_{SF} = \frac{\Delta N_{noneq}}{2}\frac{\Delta L}{\Delta t}\hat{z} = \frac{\hbar}{2}\frac{I}{e}P_I\hat{z}, \qquad (1)$$

where ΔL is the change in angular momentum.

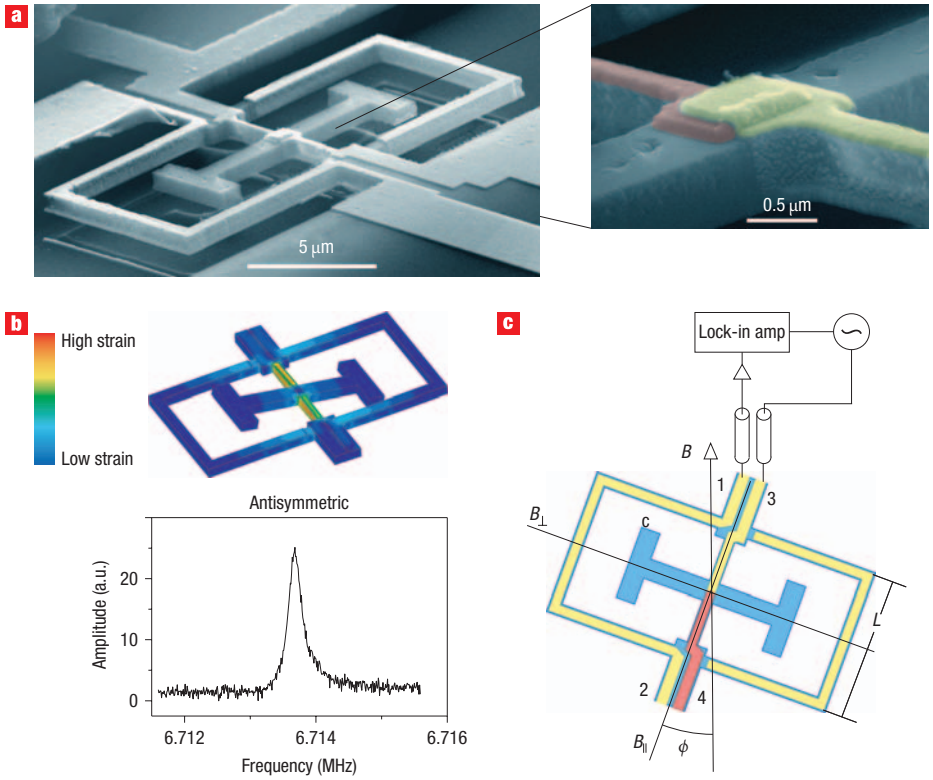

Figure 2 The spin-torsion oscillator. a, Scanning electron microscopy image of the nanomechanical device with the enlarged image showing the FM–NM interface (cobalt, red; gold, yellow). The overall dimensions of the oscillator are 12 × 6 μm with a thickness of 500 nm. The central wire is 300 nm wide, with a 50-nm-thick gold layer deposited on the NM side and 50-nm-thick cobalt layer on the FM side. The fully suspended structure is clamped rigidly at the large support pads and placed in a vacuum of 1×10^{-6} torr in a dilution refrigerator at 110 mK. **b**, Finite-element simulation of the antisymmetric torsion mode showing the colour-coded elastic strain localized on the central wire (upper part). For nearly equal rotational moments of inertia of the inner and outer torsion elements, the strain in the antisymmetric mode provides optimum amplitude coupling and minimized dissipation. The measured resonance signal (lower part) is a Lorentzian peak centred at $f_0 = 6.7137$ MHz with $Q = 28{,}000$. **c**, Setup of the measurement arrangement showing tilting of the sample with respect to the axial magnetic field B. The sample stage can be controllably tilted through an angle ϕ from 0 to 90°. The parallel component of the magnetic field polarizes the cobalt nanowire (shown in red), while the perpendicular component induces the detected signal V_{emf} in the outer electrode (yellow). The central wire is driven on resonance and the induced signal detected on the outer electrode using a lock-in amplifier.

Here, we demonstrate a nanomechanical device designed to detect and control spin-flip torque. Figure 2a shows a scanning electron micrograph of a single-crystal silicon torsion oscillator, fabricated by electron-beam lithography and surface nanomachining. The FM–NM interface is located at the junction of the cobalt and gold electrodes on the central wire. When current is driven through the interface by means of electrical connections 3–4, the spin-flip process causes localized mechanical torque because of the spin diffusion length being much smaller than the central wire length. The outer electrode 1–2 is used to detect the transverse displacement of the outer torsion element magnetomotively. The spin torque is extracted from the magnetic field dependence of the induced voltage V_{emf} on the outer electrode, which is amplified and measured by a lock-in amplifier (Fig. 2c). The torsion oscillator is mounted at the centre of a 16 T superconducting solenoid magnet on a moveable sample stage, with which it is possible to controllably tilt the sample in the plane of the oscillator. The tilt angle ϕ between the applied magnetic field and the $\hat{z}$ axis of the structure can then be varied from 0 to 90° with a precision of ±1°, as shown in Fig. 2c. The field component $B_\perp = B \sin\phi$ perpendicular to the detection electrode 1–2 is the effective field that induces the magnetomotive voltage V_{emf}. The magnetic field polarizes the central wire in the magnet, leading to polarization $P_I = P \tanh(\chi(B \pm B_0)/\mu_0 M)$, where P, χ, B_0 and M are the saturation polarization, susceptibility, coercive field and magnetization of the ferromagnet, respectively. Our measurement setup is sensitive to the polarization of the central wire along the wire axis $P_I(\phi) = P_I \cos\phi$. The sample stage and the coaxial cables are thermally anchored to the mixing chamber of a dilution cryostat in vacuum at a temperature of 110 mK. The vibration spectrum of the torsion oscillator shows two resonance peaks at 5.06 and 6.71 MHz, corresponding respectively to the symmetric and antisymmetric torsion modes with typical quality factors of $Q = 28{,}000$.

Equation (2) captures the dynamical response of the spin-torque resonator in the magnetomotive actuation–detection setup. It is derived by modelling the resonator as a damped harmonic oscillator with response contribution from the relevant modes as the oscillator is driven in the antisymmetric resonance mode by an applied current (see Supplementary Information, Section B). The induced Faraday voltage on resonance is given by

$$V(\omega_0) = \frac{-i\omega_0 L d B_\perp}{J}\left(\frac{-L d B_\perp \lambda_J}{\Omega_0^2 - \omega_0^2 + i\Gamma\omega_0} + \frac{\hbar P_I(\phi)/2e}{i\gamma\omega_0}\right) I(\omega_0). \quad (2)$$

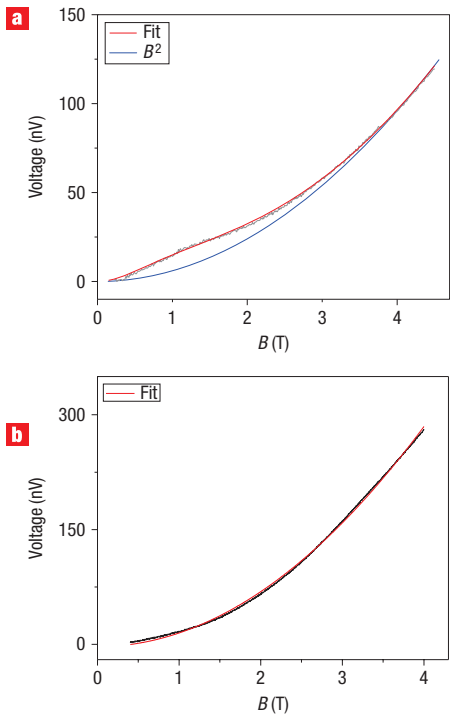

Figure 3 The response of devices with and without the FM–NM interface. Magnetic field sweeps were performed on resonance at a stage angle of $\phi = 25°$ and a current of $I = 5.5$ μA. **a**, Measurements for the gold–cobalt sample show excellent agreement with the analytical fit to the spin-torque response amplitude in equation (2) (red curve). The B^2 Lorentz response background (blue curve) is included for reference. **b**, Measurements for the cobalt control sample, containing no FM–NM interface, follow closely the expected Lorentzian response (red line fit), showing quadratic dependence on B.

Here, ω_0 is the antisymmetric mode frequency and γ the associated damping, and Ω_0 and Γ denote the fundamental flexural mode frequency and damping, respectively. J is the torsion moment of inertia of the resonator, $\lambda_J = J/Md^2$, M is the flexural modal mass of the resonator, L is the length of the portion of the outer electrode that is parallel to the central wire, and d is the distance from the central wire to the outer electrode. The first term in equation (2) results from the transverse motion of the oscillator due to the Lorentz force exerted on the central wire, and is proportional to $B_\perp^2$. The second term is the torsion response on resonance resulting from the applied spin torque and is proportional to $B_\perp$. These two terms enter in the induced voltage in a linear superposition with a phase difference of π, causing a dip in the response at magnetic field $B_\perp^* = (P_I(\phi)/4\pi)(\phi_0/L)(d\lambda_\gamma/\lambda_J)$ (see Supplementary Information, Section B). The position of the dip in the voltage amplitude is, depending on geometrical prefactors, a measure of the spin polarization. We measured the amplitude and phase of the signal $V(\omega_0)$ as a function of the applied magnetic field B, the driving current I and the tilt angle ϕ. For clarity, the model presented here does not include the capacitive crosstalk coupling between the drive and detection electrodes in our setup, the analysis of which results in a small correction to the detected voltage signal (see Supplementary Information, Section E). The amplitude of equation (2) is plotted in Fig. 1b, and we use this form to fit our detected voltage signal.

In addition to the main device having a FM–NM (cobalt–gold) interface on the central wire, we also fabricated and took

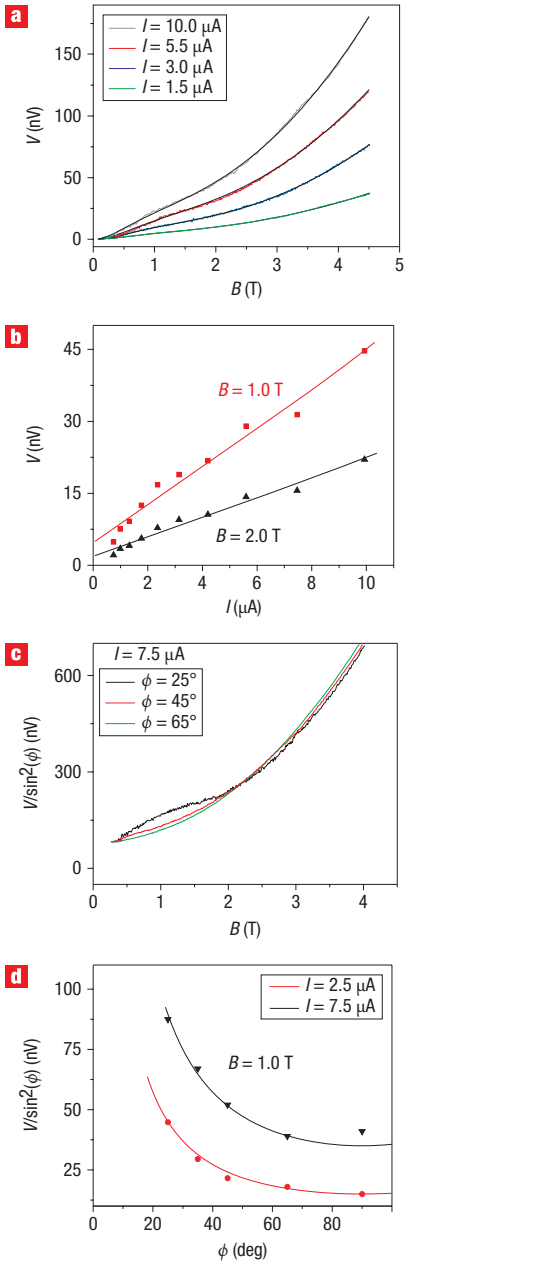

Figure 4 Voltage response for the gold–cobalt sample. a, Plot of the resonator response at various driving currents at a fixed stage angle of $\phi = 25°$. The numerical fits (amplitude of equation (2)) are shown in black. **b**, The linear current dependence of the spin torque response was verified at two values of the magnetic field, at a tilt angle $\phi = 25°$. The solid lines are guides to the eye. **c**, The Lorentz voltage response is normalized by $\sin^2\phi$ to show the variation with ϕ, and plots are shown of the response at three values of the tilt angle. At a low tilt angle of $\phi = 25°$, the applied field polarizes the ferromagnet along the wire, and the resulting spin torque is manifested as an increased torsion response in the low field range up to 2 T. Above this field range the field-dependent phase of the response in equation (2) causes the amplitude to drop below the B^2 Lorentz background. The signature of the spin torque decreases rapidly with tilt angle as the magnetization along the central wire axis decreases and the transverse field $B_\perp$ grows, moving the predicted dip in the voltage to smaller fields. **d**, Variation of the normalized resonator response with stage angle ϕ for two different driving currents, showing the vanishing of the spin-torque contribution to the signal at high tilt angles as the polarizing field $B_{||}$ vanishes. The curves are guides to the eye.

measurements for an equivalent control sample without the FM–NM interface. In the control sample, the metallic electrode on the central wire was made entirely of cobalt. Figure 3 shows the field dependence of the measured voltage amplitude for the gold–cobalt (Fig. 3a) and cobalt (Fig. 3b) samples at a stage tilt angle of $\phi = 25^\circ$. The response from the cobalt sample is due only to Lorentz force excitation and has the expected B^2 dependence. The signal from the gold–cobalt sample, on the other hand, contains a contribution from the response to the spin torque at the FM–NM interface. Use of the control sample rules out effects such as magneto-resistance or Wiedemann torque[24], which are both expected to be very small in the present experiment (see Supplementary Information, Section E).

Figure 4a plots the measured voltage amplitude for different driving currents at a stage angle of $\phi = 25^\circ$ for the gold–cobalt sample. The response varies linearly with current (Fig. 4b), as expected from equation (2). $V(\omega_0)/\sin^2\phi$ is also plotted at various stage angles ϕ in Fig. 4c,d. This normalized response approaches the B^2 Lorentz form as the central wire is tilted away from the applied field (ϕ increases) because the polarization $P_I(\phi) = P_I \cos\phi$ along the wire vanishes. At low tilt angle ϕ, where the polarization is mainly along the wire, the spin torque manifests itself through a well-predicted deviation by the theory from the quadratic field dependence of the torsion response amplitude (Fig. 4c). The typical spin-flip torque detected in our nanowire carrying a current of 1 μA is equal to 2.3×10^{-22} N-m.

From numerical fitting of the data we extracted the polarization parameter $P = 0.85 \pm 0.04$, where the error arises from the uncertainty in the estimates of the mechanical parameters. Cobalt is known to be a strong ferromagnet with all majority spin *d*-bands filled and nearly negligible spin polarization of *sp*-electrons. Therefore, we can identify the current polarization P directly with the relative contribution of *d*-electrons (see Supplementary Information, Section A). In comparison with previous experiments[27,28], ours is a novel technique for measuring P independently, as it does not involve superconducting contacts. In next-generation experiments based on our technique, the measurement of P will require a complete calibration protocol to reach a necessary level of precision.

We express our sensitivity in terms of the minimum detectable number of spins, where the associated oscillator displacement from a single spin-flip event is $x_1 = \hbar d/(2J_{SF}\gamma)$. The smallest detected signal in our experiment corresponds to 76,000 spin-flip events ($I = 0.75$ μA with an acquisition time of 1 s). To estimate the expected sensitivity of our device, we performed a detailed theoretical analysis of noise (see Supplementary Information, Sections C and D). We show that the two dominant sources of noise in our setup are the preamplifier noise (effective noise temperature $T_N = 92$ K) and the thermal noise of the mechanical mode, estimated using the classical fluctuation–dissipation theorem. The preamplifier noise and thermal noise correspond to equivalent torque noise spectral densities of $S_T^{1/2}(\text{amp}) = 5.0 \times 10^{-23}$ N-m Hz$^{-1/2}$ and $S_T^{1/2}(\text{th}) = 3.0 \times 10^{-24}$ N-m Hz$^{-1/2}$, respectively. The preamplifier noise determines our limiting sensitivity of 23,500 spin-flip events per Hz$^{1/2}$. Because our experimental setup is not perfectly optimized, it exhibits a slightly higher noise than these theoretical estimates. Significant enhancement in detector sensitivity is expected using ultralow-noise preamplifiers in our next-generation magnetometer design, with higher resonance frequencies and lower measurement temperature.

Here, we have demonstrated the detection of spin torque with a sensitivity of 1×10^{-22} N-m Hz$^{-1/2}$ in a FM–NM hybrid torsion oscillator. This level of torque sensitivity competes favourably with the 1×10^{-21} N-m Hz$^{-1/2}$ range of sensitivity in approaches for molecular torque measurements using optical tweezers. In addition, our approach paves the way to the development of new devices combining spintronics and nanomechanics, with applications from molecular torque detection and measurement[29] to nanomechanical tests of spintronics effects[30]. Future work will require improvements in fabrication, measurement and characterization, as well as the development of calibration protocols for precise quantitative analysis.

Received 27 June 2008; accepted 25 September 2008; published 2 November 2008.

References

1. Richardson, O. W. A mechanical effect accompanying magnetization. *Phys. Rev.* **26,** 248–253 (1908).
2. Einstein, A. & de Hass, W. J. Experimenteller Nachweis der ampere'schen molekularstroeme. *Verhandlungen der Deutschen Physikalischen Gesellschaft* **17,** 152–170 (1915).
3. Beth, R. A. Mechanical detection and measurement of the angular momentum of light. *Phys. Rev.* **50,** 115–125 (1936).
4. Barnett, S. J. New researches in gyromagnetism. *Phys. Rev.* **66,** 224–225 (1944).
5. Kittel, C. On the gyromagnetic ratio and spectroscopic splitting factor of ferromagnetic substances. *Phys. Rev.* **76,** 743–748 (1949).
6. Scott, G. G. A precise mechanical measurement of the gyromagnetic ratio of iron. *Phys. Rev.* **82,** 542–547 (1952).
7. Wallis, T. M., Moreland, J. & Kabos, P. Einstein-de Haas effect in a NiFe film deposited on a microcantilever. *Appl. Phys. Lett.* **89,** 122502 (2006).
8. Ascoli, C. *et al.* Micromechanical detection of magnetic resonance by angular momentum absorption. *Appl. Phys. Lett.* **69,** 3920–3922 (1996).
9. Slonczewski, J. C. Current-driven excitation of magnetic multilayers. *J. Magn. Magn. Mater.* **159,** L1–L7 (1996).
10. Berger, L. Emission of spin waves by a magnetic multilayer traversed by a current. *Phys. Rev. B* **54,** 9353–9358 (1996).
11. Sun, J. Z. Current-driven magnetic switching in manganite trilayer junctions. *J. Magn. Magn. Mater.* **202,** 157–162 (1999).
12. Myers, E. B., Ralph, D. C., Katine, J. A., Louie, R. N. & Buhrman, R. A. Current-induced switching of domains in magnetic multilayer devices. *Science* **285,** 867–870 (1999).
13. Tsoi, M. *et al.* Generation and detection of phase-coherent current-driven magnons in magnetic multilayers. *Nature* **406,** 46–48 (2000).
14. Wegrowe, J.-E. *et al.* Exchange torque and spin transfer between spin-polarized current and ferromagnetic layers. *Appl. Phys. Lett.* **80,** 3775–3777 (2002).
15. Stiles, M. D. & Zangwill, A. Anatomy of spin-transfer torque. *Phys. Rev. B* **65,** 014407 (2002).
16. Pospelov, M. & Romanis, M. Lorentz invariance on trial. *Physics Today* **40,** 40–46 (July 2004).
17. Heckel, B. R. *et al.* New CP-violation and preferred-frame tests with polarized electrons. *Phys. Rev. Lett.* **97,** 021603 (2006).
18. Bryant, Z. *et al.* Structural transitions and elasticity from torque measurements on DNA, *Nature* **424,** 338–341 (2003).
19. Noji, H., Yasuda, R., Yoshida, M. & Kinosita, K. Direct observation of the rotation of F1-ATPase. *Nature* **386,** 299–302 (1997).
20. Ryu, W. S., Berry, R. M. & Berg, H. C. Torque-generating units of the flagellar motor of *Escherichia coli* have a high duty ratio. *Nature* **403,** 444–447 (2000).
21. Johnson, M. & Silsbee, R. H. Thermodynamic analysis of interfacial transport and of the thermomagnetoelectric system. *Phys. Rev. B* **35,** 4959–4972 (1987).
22. Johnson, M. & Silsbee, R. H. Coupling of electronic charge and spin at a ferromagnetic–paramagnetic metal interface. *Phys. Rev. B* **37,** 5312–5325 (1988).
23. Fabian, J. & Das Sarma, S. Spin relaxation of conduction electrons. *J. Vac. Sci. Technol. B* **17,** 1708–1715 (1999).
24. Mohanty, P., Zolfagharkhani, G., Kettemann, S. & Fulde, P. Spin-mechanical torsion device for detection and control of spin by nanomechanical torque. *Phys. Rev. B* **70,** 195301 (2004).
25. Kovalev, A. A., Bauer, G. E. W. & Brataas, A. Current-driven ferromagnetic resonance, mechanical torques and rotary motion in magnetic nanostructures. *Phys. Rev. B* **75,** 014430 (2007).
26. Fulde, P. & Kettemann, S. Spin-flip torsion balance. *Ann. Phys.* **7,** 214–216 (1998).
27. Upadhyay, S. K., Palanisami, A., Louie, R. N. & Buhrman, R. A. Probing ferromagnets with Andreev reflection. *Phys. Rev. Lett.* **81,** 3247–3250 (1998).
28. Soulen, R. J. *et al.* Measuring the spin polarization of a metal with a superconducting point contact. *Science* **282,** 85–88 (1998).
29. Volpe, G. & Petrov, D. Torque detection using brownian fluctuations. *Phys. Rev. Lett.* **97,** 210603 (2006).
30. Weiss, P. Magnetic overthrow. *Science News* **169,** 11–13 (2006).

Supplementary Information accompanies this paper at www.nature.com/naturenanotechnology.

Acknowledgements

This work was primarily supported by the National Science Foundation (Division of Material Research (DMR)-0346707) under the NSF-European Community (EC) Cooperative Activity in Materials Research (Material World Network). S.K. acknowledges support by the Deutsche Forschungsgemeinschaft (DFG) (Sonderforschungsbereich (SFB)668 B3 and DFG SFB508 B9). P.D. acknowledges support from the Condensed Matter Theory visitors program at Boston University, the Centre National de la Recherche Scientifique/Direction des Relations Internationales (CNRS/DREI) (contract no. 4024) and Agence Nationale pour la Recherche (ANR)-PNANO Quspin. The authors thank M. Johnson, I. Zutic, T. Wehling, J. Wei, L. Saminadayar, C. Bäuerle and C. Chamon for helpful discussions.

Author contributions

All authors discussed the results and commented on the manuscript.

Author information

Reprints and permission information is available online at http://npg.nature.com/reprintsandpermissions/.
Correspondence and requests for materials should be addressed to P.M.